140 KSME Journal, Vol. 6, No. 2, pp. 140~148, 1992

NUMERICAL CALCULATION OF THE VISCOUS FLOW AROUND A ROTATING MARINE PROPELLER

Keon-Je Oh* and Shin-Hyoung Kang**

(Received June 1, 1992)

Reliable and accurate prediction of the viscous flow around a marine propeller operating at the stern is of practical importance for design and performance prediction of propellers. A computer code was developed in the present study for the full viscous flow simulation around the marine propeller at the stern and its performance was investigated using the available data. The continuity and Navier-Stokes equations with a standard k-ε model in the rotating coordinate fixed on the propeller were numerically solved using FVM. The predicted profiles of circumferentially averaged velocity and turbulent kinetic energy were in accordance with the measured data at the downstream of the propeller, while there were significant discrepancies in the near wake. The value of velocity was small in a core associated with the formation of the tip vortex and the location of maximum axial velocity on the suction side of the blade was observed in the simulation. The flow structure observed in the experiment was confirmed in the simulation, however not quantitatively. The blade wake was diffused more in comparison with the measured one.

Key Words: Propeller, k-ε Model, Control Volume Method

NOMENCLATURE

a_i	: Coefficients in the descretized Eq.
b_j^i	: Transformation matrix
C_μ, C_D, C_1, C_2	: Turbulence model constants
D_p	: Diameter of the propeller
E	: Constant
J	: Jacobian
k	: Turbulent kinetic energy
L	: Body length
m	: Mass flow rate
N	: Rotational speed of the propeller
n	: Normal distance from the surface
M_{xx}	: Axial momentum deficit parameter
$M_{\theta x}$	: Tangential momentum parameter
P	: Pressure
R_e	: Radius of the external boundary
R_h	: Radius of the hub
R_p	: Radius of the propeller
S_ϕ	: Source term for each variable
U, V, W	: Velocity components in x, r, θ dir.
x, r, θ	: Cylindrical coordinates
ε	: Dissipation rate of kinetic energy
ϕ	: Specific variable
Γ_ϕ	: Diffusion coefficient of ϕ
$\varkappa$	: Von Karman constant
ρ	: Density
σ_k, σ_ε	: Turbulence model constants
τ_w	Wall shear stress
ω	: Rotational speed of the propeller
ξ, η, ς	: Boundary fitted coordinates

*Department of Mechanical Engineering, Kyungnam University, Masan, Korea 630-701
**Department of Mechanical Engineering, Seoul National University, Kwanak Ku, Seoul, Korea 151-742

1. INTRODUCTION

Modern propeller design methods are mainly based on the inviscid flow theory, with various viscous effects taken into account only through empirical information concerning blade drag and wake. The hull and propeller interaction, which is also one of the most important phenomena to understand the ship propulsion efficiency, is strongly influenced by viscous effects. Reliable and accurate prediction of the viscous flow around a marine propeller operating at the stern is of practical importance for design and performance prediction of propellers. The function and geometry of a propeller are similar to those of general turbomachines, but the flow features become more complicated due to unsteadiness, three-dimensionality, and high level of turbulence. It is also still difficult job to reasonably simulate the vortex type of flow near the tip and the hub.

Various numerical methods have been developed in the past for the two or three dimensional flows, compressible or incompressible flows, inviscid or viscous flows, and steady or unsteady flows. Techniques for turbomachinery flow computations have reached a high level of maturity. However, there is still a need of calibration of the computation even for the two-dimensional cascade flow (Kang et al., 1992). Only a few cases of viscous flow simulation of marine propeller have been reported in the past. Recently, Stern and Kim(1990) presented the calculated results of the flow through a propeller with rectangular blades using Navier-Stokes analysis.

On the other hand, very little information is available on the details of the unsteady, turbulent flow behind a body-propeller combination, not only for the physical understanding of the flow structure but also the assessment numerical methods. The measurement of the flow around a propeller is very difficult to carry out in the rotating blades as well as in

the wake. Recently, Hyun(1991) and Hyun and patel(1991 a, b) experimentally investigated the flow behind a propeller operating on the axisymmetric body in the wind tunnel. They reported interesting features of the propeller wake and provided extensive data, i.e. circumferentially averaged and 3-dimensional phase averaged values of mean velocity components and Reynolds stresses. Any numerical investigations for the above measurements are not reported yet.

The objectives of the present study are to develop a computer code for the three-dimensional viscous flow simulation around the marine propeller at the stern and investigate the performance using the available data of Hyun and Patel(1991 a, b). The continuity and Navier-Stokes equations with a standard k-ε model were solved using a Finite Volume method. The simulated results are discussed below.

2. FORMULATION

2.1 Governing Equations

Configuration of the propeller mounted on the axisymmetric stern is shown in Fig. 1. The governing equations for the incompressible, steady, and turbulent flow are given by the continuity and the Reynolds averaged Navier-Stokes equations. They are written in the rotating cylindrical coordinate system (x, r, θ) fixed on the propeller blade of constant angular velocity ω. Reynolds stresses are modelled using a standard k-ε model. The values of k and ε are obtained from their transport equations. Modified versions of k-ε model for low-intensity turbulence, anisotropic turbulence, rotating effects on turbulence, etc. have been investigated. Since they are not well developed yet for the general purposes, a simple standard k-ε model is used in this study. The general form of the governing equations can be written as follows,

$$\frac{\partial}{\partial x}(U\phi)+\frac{1}{r}\frac{\partial}{\partial r}(rV\phi)+\frac{1}{r}\frac{\partial}{\partial\theta}(W\phi)=\frac{\partial}{\partial x}\left[\Gamma_\phi\frac{\partial\phi}{\partial x}\right]+\frac{1}{r}\frac{\partial}{\partial r}\left[r\Gamma_\phi\frac{\partial\phi}{\partial r}\right]+\frac{1}{r^2}\frac{\partial}{\partial\theta}\left[\Gamma_\phi\frac{\partial\phi}{\partial\theta}\right]+S_\phi \quad (1)$$

where ϕ, Γ_ϕ, and S_ϕ denote the flow variables, diffusion coefficients and source terms respectively (cf. Table 1).

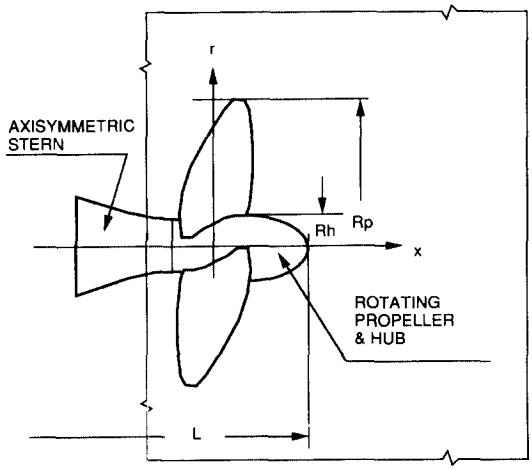

Fig. 1 Configuration of a body-propeller, flow domain for simulation and cylindrical coordinate

2.2 Transformation of Governing Equations

The flow domain is schematically shown in Fig. 1, which is bounded by the propeller blade passage, the propeller hub and body surfaces, the axis of wake, the upstream and downstream sections, and the outer boundary. A non-orthogonal body-fitted coordinate system(ξ, η, ζ) is used to transform the physical domain to a rectangular computational domain. The transformation of the independent variables (x, r, θ) in the governing equations leaving the flow variables ϕ in the original cylindrical coordinate, can be expressed as follows (Kang et al., 1991, Oh and Kang, 1992)

$$\frac{\partial}{\partial\xi}(b_1^1U\phi+b_2^1V\phi+b_3^1W\phi)+\frac{\partial}{\partial\eta}(b_1^2U\phi+b_2^2V\phi+b_3^2W\phi)+\frac{\partial}{\partial\zeta}(b_1^3U\phi+b_2^3V\phi+b_3^3W\phi)=\frac{\partial}{\partial\xi}\left[\Gamma_\phi Jg^{11}\frac{\partial\phi}{\partial\xi}\right]+\frac{\partial}{\partial\eta}\left[\Gamma_\phi Jg^{22}\frac{\partial\phi}{\partial\eta}\right]+\frac{\partial}{\partial\zeta}\left[\Gamma_\phi Jg^{33}\frac{\partial\phi}{\partial\zeta}\right]+S_\phi \quad (2)$$

where b_j^i is the transformation matrix which is represented by the partial derivatives of (x, r, θ) with respect to (ξ, η, ζ). J is Jacobian, g^{ij} is metric tensor, and S_ϕ is the source term in the transport equation for each variable.

2.3 Boundary Conditions

Boundary conditions imposed on each boundary are as follows:

(1) Upstream section; The values of the 3 components of velocity and the turbulent kinetic energy and its dissipation rate are prescribed. The pressure is not required, since the staggered grid system is chosen in the present calculation. Determination of the upstream condition is dependent on the interaction between the hull and the propeller. A simple viscous flow calculation is carried out to determine the boundary conditions, for the extended region around the axisymmetric body with the propeller modelled by the uni-

Table 1 ϕ, Γ_ϕ, and S_ϕ in the governing equations

ϕ	Γ_ϕ	S_ϕ
1	0	0
U	ν_e	$-\frac{1}{\rho}\frac{\partial P}{\partial x}+\frac{\partial}{\partial x}\left[\nu_t\frac{\partial U}{\partial x}\right]+\frac{1}{r}\frac{\partial}{\partial r}\left[r\nu_t\frac{\partial V}{\partial x}\right]+\frac{1}{r}\frac{\partial}{\partial\theta}\left[\nu_t\frac{\partial W}{\partial x}\right]$ $-\frac{1}{r}\frac{\partial P}{\partial r}+\frac{\partial}{\partial x}\left[\nu_t\frac{\partial U}{\partial r}\right]+\frac{1}{r}\frac{\partial}{\partial r}\left[r\nu_t\frac{\partial V}{\partial r}\right]+\frac{1}{r}\frac{\partial}{\partial\theta}\left[\nu_t\frac{\partial W}{\partial r}\right]$
V	ν_e	$-\frac{1}{r^2}\frac{\partial}{\partial\theta}(\nu_tW)-\frac{2\nu_e}{r^2}\frac{\partial W}{\partial\theta}-\nu_e\frac{V}{r^2}-\nu_t\frac{V}{r^2}+\frac{W^2}{r}+r\omega^2+2\omega W$ $-\frac{1}{\rho r}\frac{\partial P}{\partial\theta}+\frac{\partial}{\partial x}\left[\frac{\nu_t}{r}\frac{\partial U}{\partial\theta}\right]+\frac{1}{r}\frac{\partial}{\partial r}\left[\nu_t\frac{\partial V}{\partial\theta}\right]$
W	ν_e	$+\frac{1}{r}\frac{\partial}{\partial\theta}\left[\frac{\nu_t}{r}\frac{\partial W}{\partial\theta}\right]-\frac{1}{r}\frac{\partial}{\partial r}(\nu_tW)+\frac{2}{r}\frac{\partial}{\partial\theta}\left[\frac{\nu_t}{r}V\right]-\nu_e\frac{W}{r^2}$ $-\frac{VW}{r}+\frac{\nu_t}{r}\frac{\partial W}{\partial r}+\frac{\nu_t}{r^2}\frac{\partial V}{\partial\theta}-2\omega V$
k	$\frac{\nu_e}{\sigma_k}$	$G-C_D\varepsilon$
ε	$\frac{\nu_e}{\sigma_\varepsilon}$	$\frac{\varepsilon}{k}(G-C_D\varepsilon)$

note: $G=\left[2\left\{\left[\frac{\partial U}{\partial x}\right]^2+\left[\frac{\partial V}{\partial r}\right]+\left[\frac{1}{r}\frac{\partial W}{\partial\theta}+\frac{V}{r}\right]^2\right\}+\left[\frac{\partial U}{\partial r}+\frac{\partial V}{\partial x}\right]^2+\left[\frac{1}{r}\frac{\partial U}{\partial\theta}+\frac{\partial W}{\partial x}\right]^2+\left[\frac{1}{r}\frac{\partial V}{\partial\theta}+\frac{\partial W}{\partial r}-\frac{W}{r}\right]^2\right]$

$\nu_e=\nu+\nu_t$, $\nu_t=C_\mu\frac{k^2}{\varepsilon}$

$C_\mu=0.09$, $C_D=1.0$, $C_1=1.44$, $C_2=1.92$, $\sigma_k=1.0$, $\sigma_e=1.3$

form distribution of momentum source corresponding to the propeller thrust.

(2) Downstream section; The downstream section is located far from the body and the propeller, and zero gradient condition is assumed for all variables.

(3) Blade and hub surfaces; To avoid the difficulty in resolving the near wall turbulent flow, the wall function is used at the surface. The grid points next to the wall are located in the fully trubulent layer where the logarithmic law is satisfied and the velocity vectors are assumed to be collateral. Then the wall shear stress τ_w and the turbulence quntities at the wall are estimated as follows

$$\frac{\tau_w}{\rho}=\varkappa V_t C_\mu^{1/4}\frac{\sqrt{k}}{\ln(E\cdot n^+)},\quad k=\frac{\tau_w}{\rho\sqrt{C_\mu}},\quad \varepsilon=\frac{C_\mu^{3/4}k^{3/2}}{\varkappa\cdot n} \tag{3}$$

where V_t is the magnitude of the velocity at the first grid point from the wall, n is the normal distance from the wall, and $\varkappa$ and E are 0.42 and 9.793 respectively.

(4) External boundary; It is placed sufficiently far from the propeller. Uniform free stream without turbulence is assumed there.

$$U=U_o,\ W=-\omega R_e,\ k=\varepsilon=0,\ P=P_o \tag{4}$$

The value of radial velocity at the external boundary is determined from thd continuity equation.

(5) Periodic surfaces; Periodic boundary conitions are enforced on the periodic surfaces.

3. NUMERICAL SCHEME

The governing equations are discretized using the Finite Volume Method and the hybrid scheme for the convective terms in the staggered grid system (Patankar, 1980). The scalar variables P, k, ε are located at grid nodes, while velocity components are placed between scalar nodes. Such a grid system has a benefit of having the velocity at the boundaries of the scalar cell where integration of the convection term is necessary. Furthermore, it is easy to calculate the pressure gradient term in the momentum equations, since the pressure nodes are located on both sides of the velocity node. The final form of the discretized equations can be expressed as below (Kang et al., 1991, Oh and Kang, 1992, Patankar, 1980).

$$a_P\phi_P=a_N\phi_N+a_S\phi_S+a_E\phi_E+a_W\phi_W+a_D\phi_D+a_U\phi_U+\overline{S}_\phi \tag{5}$$

The subscript P refers to a grid node to be considered and the subscripts U, D correspond to the upstream and downstream grid points respectively. The neighbouring grid points in the section are denoted by N, S, E, W, and a_N, a_S, a_E, a_W, etc. represent the diffusion and convection coefficients at each corresponding surface of the control volume.

Since the velocity field obtained using the previous values of pressure at each iteration does not satisfy the continuity equation, they are corrected using the corrected values of pressure, which are obtained using the continuity equation, i.e. the SIMPLE algorithm (Patankar, 1980). The discretized form of pressure correction equation is obtained in the form of Eq. (5).

4. CALCULATIONS

4.1 Model Propeller

The developed numerical method is applied to the propeller investigated by Hyun(1990) and Hyun and Patel(1991 a, b) in the wind-tunnel. The propeller was mounted at the stern of an axisymmetric body, which was designed modifying the Afterbody 5 of Huang et al.(1980). The total length is $L=151.61$ cm. The diameter of the propeller is $D_p=2R_p=10.16$ cm, and the hub-tip ratio of the propeller is $R_h/R_p=0.2187$. The propeller has three blades, the sections of which have NACA-66 thickness distributions. It was mounted at $x/L=0.9755$. The value of the freestream velocity and the number of rotations were $U_0=16.5$ m/s, $N=200$ rps respectively. The Reynolds numbers based on the body length and the chord length at $r/R_p=0.7$ of the propeller blade were 1.55×10^6 and 1.44×10^5.

Extensive measurements were carried out at the down stream of the propeller using a five hole pitot tube and a hot-wire anemometer. Measured data, i.e. mean velocities, static pressures, turbulent kinetic energies, and Reynolds stresses are available for the assessment of the present numerical study.

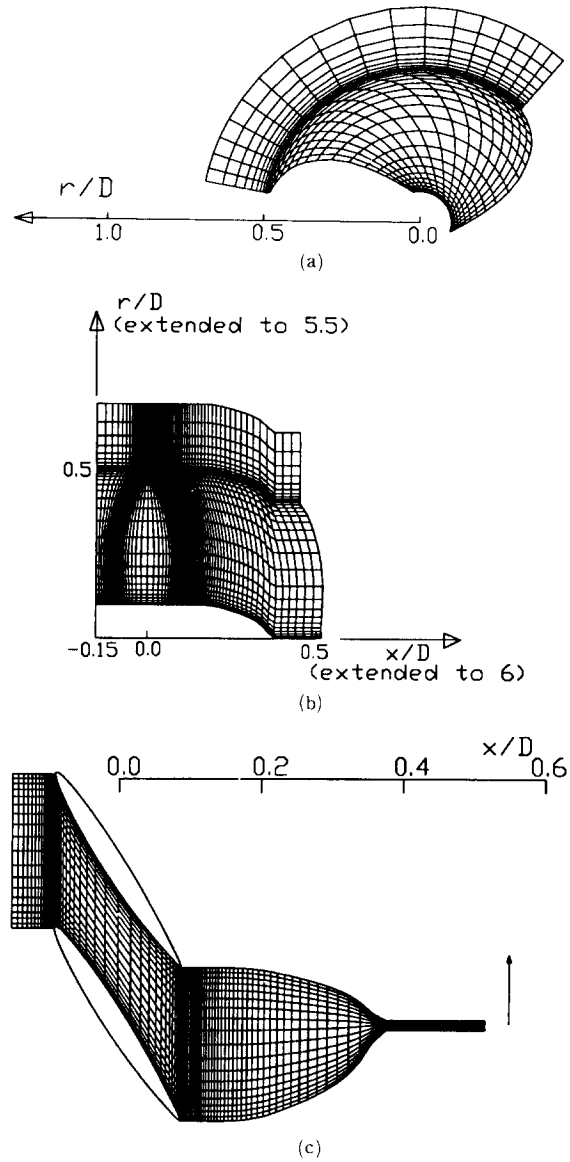

Fig. 2 Parts of the generated mesh on (a) $\xi=1.0$, (b) $\eta=2.0$, (c) $\zeta=1.0$ planes

4.2 Grid Generation and Estimation of Inlet Conditions

Since the propeller operates at the stern, the calculation domain should cover the whole field of the flow including the body as well as the propeller. However, the number of grid point is still limited by the computer capacity and the main interest of the present study is to simulate the flow near the propeller. The computational grid was algebraically generated in the limited domain, which is bounded by two neighbouring blades, the sections of $x/D_p=-0.15$ at the upstream and of $x/D_p=6.0$ at the downstream locations. The external boundary is located at $r/D_p=5.5$, which is far enough from the propeller. The numbers of grid point were 132, 40, and 20 in the streamwise, radial, and circumferential (blade-to-blade) directions respectively. The finer meshes are allocated near the leading and trailing edges, propeller tip, and the blade and body surfaces considering rapid changes in the velocity. The generated meshes at the $\xi=1$, $\eta=2$, and $\zeta=1$ surfaces are shown in Fig. 2.

Since the inlet section of $x/D_p=-0.15$ locates near the propeller, the flow is strongly distorted due to the body and propeller interaction. The boundary conditions, i.e. the values of each velocity components and the turbulent kinetic energy and its dissipation rate should be properly estimated there. These values were estimated by axisymmetric viscous flow calculation with coarse grids over the whole domain including the body and the propeller. The interaction of the body and the propeller was taken into account in the calculation, assumming the acting propeller to be the uniformly distributed momentum source corresponding to the propeller thrust.

The calculated streamwise and radial components of velocity at the inlet position with and without the propeller are compared with measured values in Figs. 3 and 4. The flow near the body is axially accelerated and radially inward motion is induced due to the propeller suction effect. The streamwise component of velocity is reasonably predicted in comparison with measured values, except near the tip of the propeller.

Solutions are assumed to be converged when the residual sources of each variable reduce to 1% of the reference value, and the converged solution is obtained after about 1000 iterations and CPU time of 5.5 hours on CRAY-2S supercomputer.

5. RESULTS AND DISCUSSION

The circumferentially averaged values of pressure coefficient along the hub and the wake center line are presented and compared with measured values in Fig. 5. The pressure ahead of the propeller is higher than the ambient pressure due to the deceleration of flow over the stern and rapidly increases through the propeller. The pressure significantly changes over the tail and in the wake. After rapid decrease in pressure due to the propeller, the pressure increases again up to the stagnation point at the tail. It monotonically recovers the ambient pressure in the wake, however the measured value recovers after showing the minimum value at $x/L=1.08$(Fig. 5). The reason of the discrepancy is not clear, however, the flow acceleration and rotational effects of the propeller and the hub may not be fully taken into accout in the simulation. Figs. 6 and 7 show the distributions of pressure coefficient in the blade to blade surfaces of the hub and $r/R_p=0.7$, respectively. The staganation point appears near

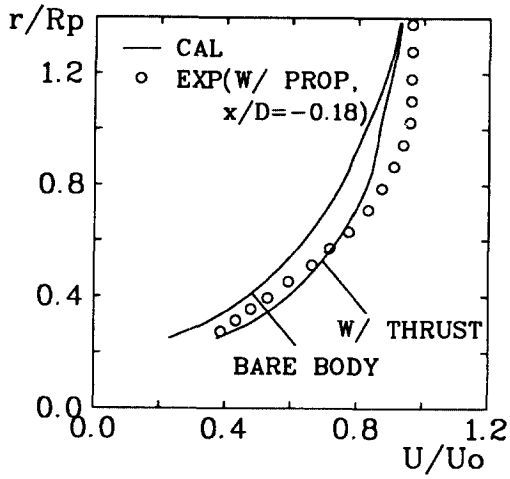

Fig. 3 Streamwise veloity components at the inlet with and without the propeller

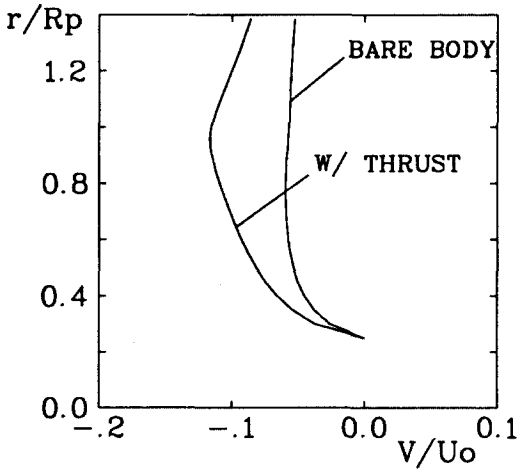

Fig. 4 Radial components of velocity at the inlet with and without the propeller

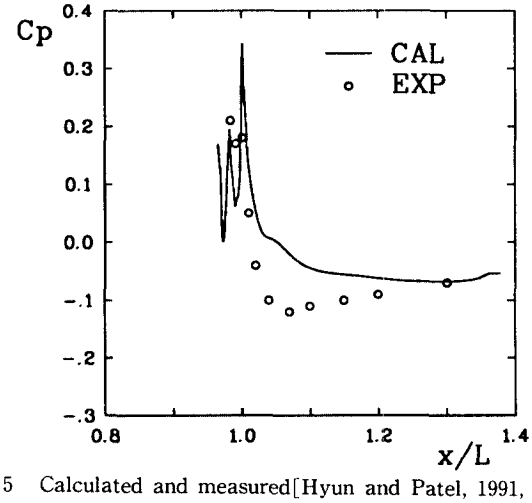

Fig. 5 Calculated and measured[Hyun and Patel, 1991, a] circumferentially averaged values of pressure coefficient along the hub and wake center line

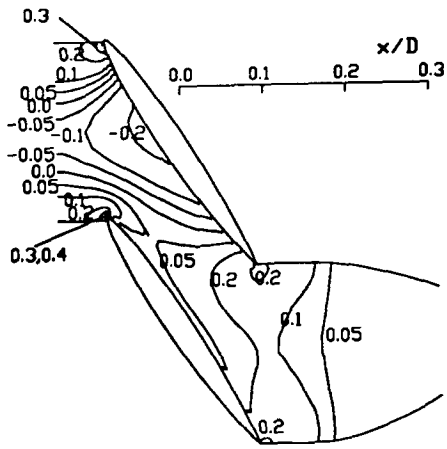

Fig. 6 Contours of equi-pressure coefficient on the blade to blade surface of the hub

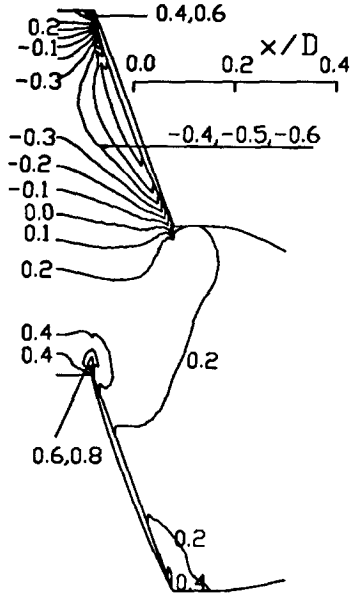

Fig. 7 Contours of equi-pressure coefficient on the blade to blade surface of $r/R_p=0.7$

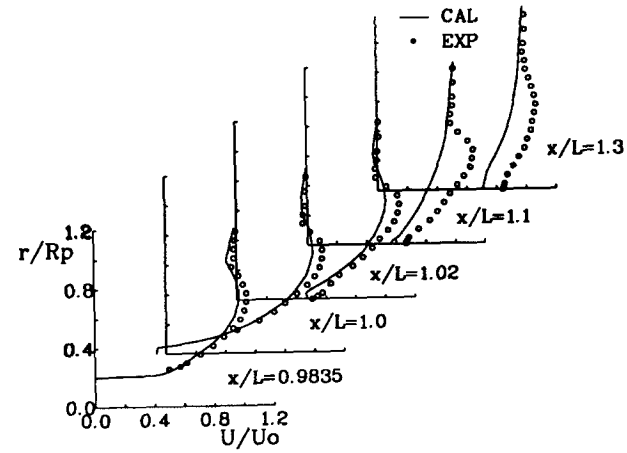

Fig. 8 Calculated and measured[Hyun and Patel, 1991 a] circumferentially averaged profiles of axial velocity compenent

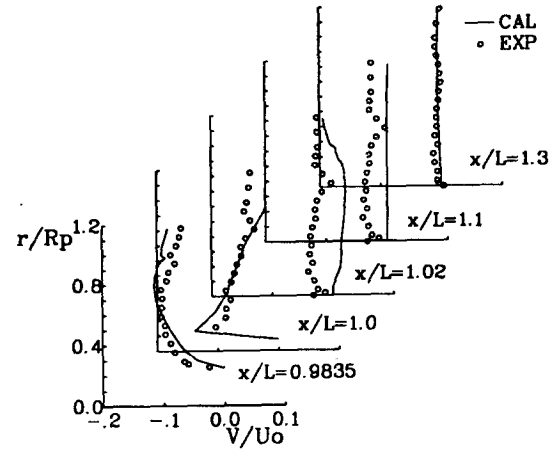

Fig. 9 Calculated and measured[Hyun and Patel, 1991 a] circumferentially averaged profiles of radial velocity compenent

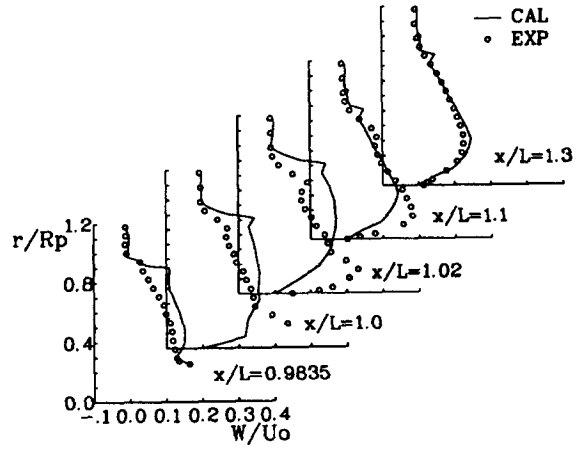

Fig. 10 Calculated and measured[Hyun and Patel, 1991 a] profiles of tangential velocity compenent

the leading edge of the pressure side. The pressure variations over the pressure side of the blade are not large. However. there appears strong adverse pressure gradient over the suction side. The location of the minimum pressure on the suction side moves to the trailing edge as the radial distance increases.

Circumferentially averaged values of mean velocity at the downstream of the propeller are compared with measured values in Figs. 8, 9 and 10. The axial acceleration of flow due to the propeller is observed in the axial velocity profiles at $x/L=0.9835$, 1.0, 1.02 in Fig. 8. The axial velocities have their maximum values at $r/R_p=0.7$, and approaches to the free stream velocity. At the tail of the body, $x/L=1.0$, a small separation region is observed in the prediction. Comparison of the predicted with the measured velocity profiles shows a reasonable coincidence up to the one diameter downstream of the propeller, while there are significant discrepancies in the

wake. At $x/L=1.1$. and 1.3, the flow still has the accelerated effect in the axial velocity due to the propeller action, however, the prediction does not show this feature in the near wake. As mentioned before, it is because the flow acceleration and rotational effect of the propeller and the hub may be not fully taken into accout in the simulation. Radial velocity profile at $x/L=0.983$ shown in Fig. 9 has its maximum value at $r/R_p=0.75$. At $x/L=0.983$ and 1.0, the predicted values show good agreement with the measured profiles and rapid change in the radial velocity was simulated near the hub. At $x/L=1.02$ and 1.1, the small values of radial component of velocity (negative in the measurement) are the consistent with the underestimation of axial velocity profile. Averaged values of swirl velocity are reasonably predicted in comparison with the measured profiles in Fig.10. The rapid variation of swirl velocity near the tip accords with the measurements. The magnitude of circumferential velocity increases from the outside to the hub like a free vortex of flow, however, they reduce to zero on the body surface and the centerline of the wake.

Averaged distributions of turbulent kinetic energy are compared with measured profiles in Fig. 11. At the just downstream of the propeller, the turbulent kinetic energy distribution was nicely calculated and showed its maximum value at the location of maximum axial velocity. This is due to the large value of generation rate of the turbulent kinetic energy over this region. However, in the downstream of the wake, the predicted values are considerbly smaller than the measured values. The standard form of k-ε model may not be adequate for this swirling flow in the downstream.

Momentum deficit parameters in the wake are useful to estimate the propeller thrust and torque. Integral parameters for the mass and momentum deficits are defined as follows

$$m=\frac{2\pi\rho}{U_oL^2}\int_0^{\delta}(U_o-U)\,rdr \tag{6}$$

$$M_{xx}=\frac{2\pi\rho}{U_o^2L^2}\int_0^{\delta}U(U_o-U)\,rdr \tag{7}$$

$$M_{\theta x}=\frac{2\pi\rho}{U_o^2L^2}\int_0^{\delta}UWrdr \tag{8}$$

The esimated values of the parameters and measured ones are presented in Fig. 12. The mass and axial momentum deficits rapidly decrease in the near wake and gradually

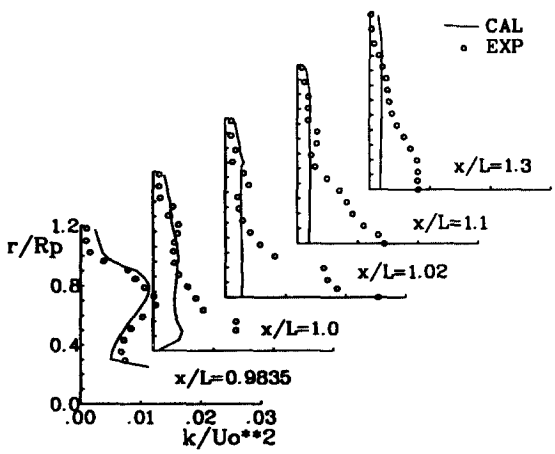

Fig. 11 Calculated and measured[Hyun and Patel, 1991 a] circumferentially averaged profiles of turbulent kinetic energy

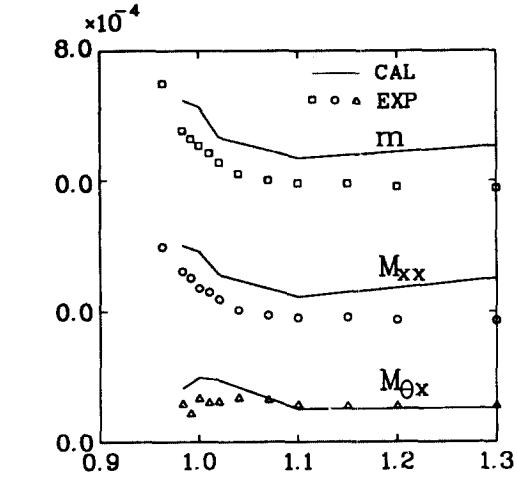

Fig. 12 Variations of mass and momentum deficit parameters

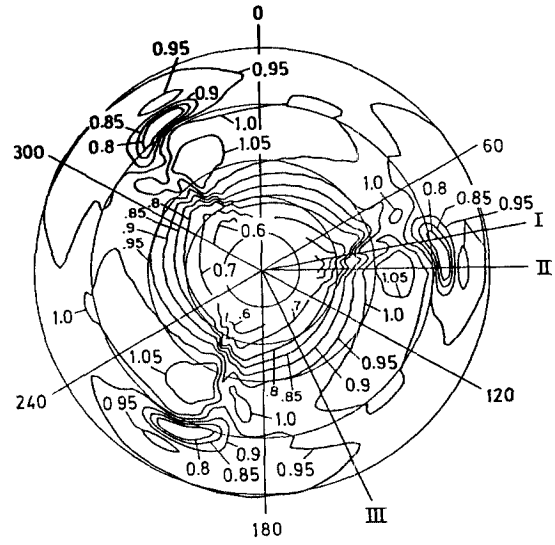

(a) measured [Hyun and Patel, 1991 b]

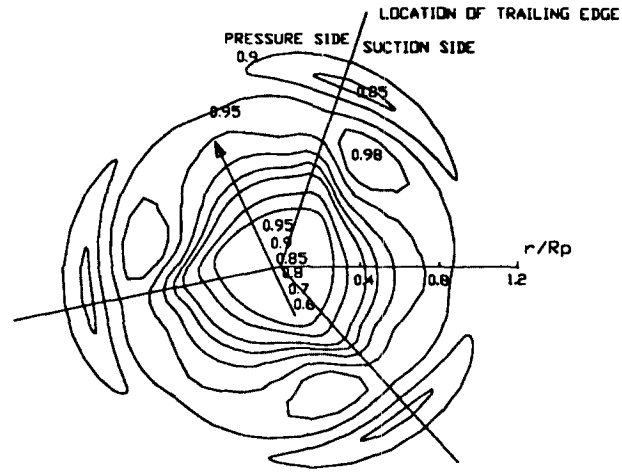

(b) calulated values

Fig. 13 Axial velocity distributions at $x/L=0.9835$

decrease to have asymptotic values in the far wake. On the other hand, the circumferential momentum generated by the swirling flow remains constant in the wake. The values of mass and axial momentum deficits from the prediction are somewhat higher than those of the measurements. This discrepancy is partially due to the difference between the estimated and measured values of the inlet boundary conditions. Over-all simulation errors are accumulated in these integral parameters. Considering the error in the parameters at the inlet location, the prediction error is not so significant.

Measurements of three-dimensional phase-averaged mean velocity field and Reynolds stresses were made with a triple hot wire sensor (Hyun, 1990, Hyun and Patel, 1991 a, b). They provided the information of complexity of the flow and contribution of local aspects of the flow in the blade wake, at the intersection of the hub and the blade as well as near the tip. The calculated and measured axial velocity contours at $x/L=0.983$ are shown in Fig. 13. Measurement shows a votex-like core with low velocity near $r/R_p=0.96$, which is associated with the formation of the tip vortex. The wake of the main span of the propeller appears in the region between 75 to 90 degrees in the phase plane. The location of maximum axial velocity was observed on the suction side and was indicated by a core of high velocity around 95 degree and $r/R_p=0.96$, where the propeller was designed to produce maximum circulation. All the aspects of the flow are confirmed in the simulation. However, the minimum value of velocity in the tip vortex is 0.85 (the measured value was 0.80) and the maximum value of velocity in the main core is 0.98 (the measured value was 1.05). The rapid changes in axial velocity across the blade wake observed in the experiment do not appear in the calculation. The projection of velocity vector at the section is presented in Fig. 14. Outside the blade wake, the radial velocity is generally negative. Within the blade wake, the radially inward motion on the suction side and outward motion on the pressure side were observed. The simulated variation of radial velocity is in accordance with the measurement. However, the weak outward motion was predicted on the pressure side. The swirling velocity rapidly reduces near the tip, however, the formation of the hub and tip vortex

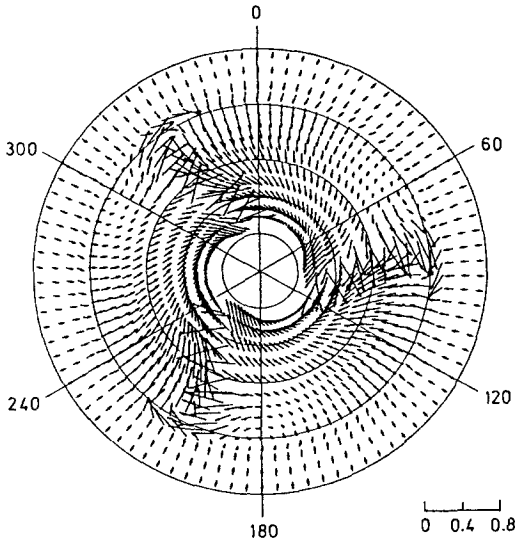

(a) measured[Hyun and Patel, 1991 b]

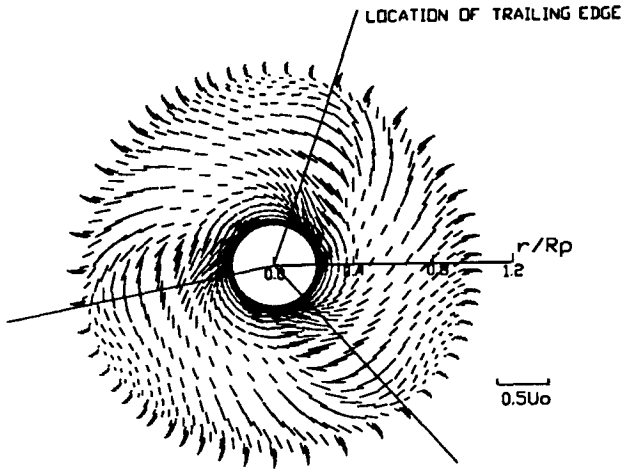

(b) calulated values

Fig. 14 Vetor plots of cross flow at $x/L=0.9835$

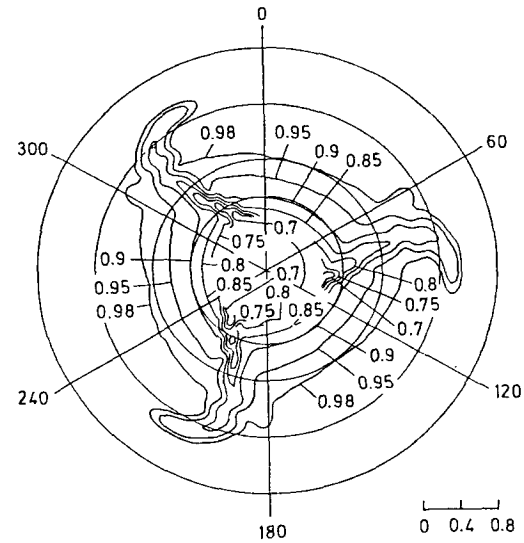

(a) measured[Hyun and Patel, 1991 b]

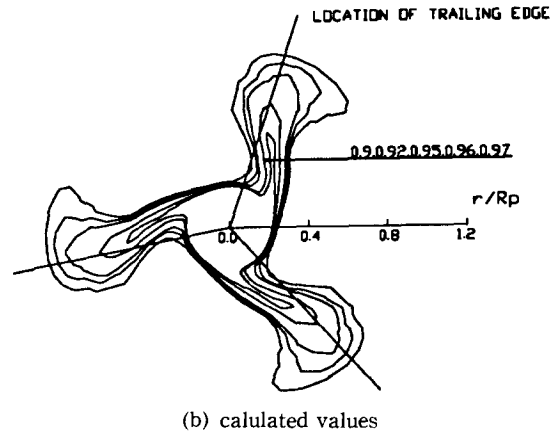

(b) calulated values

Fig. 15 Streamwise velocity contours at $x/L=0.9835$ in moving pitchline coordinate

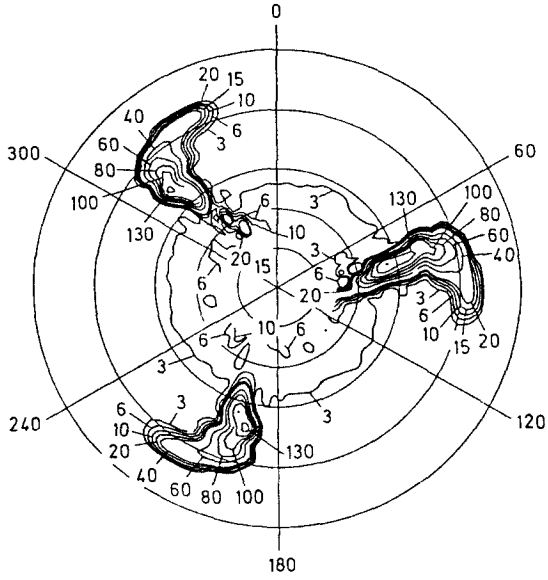

(a) measured[Hyun and Patel, 1991 b]

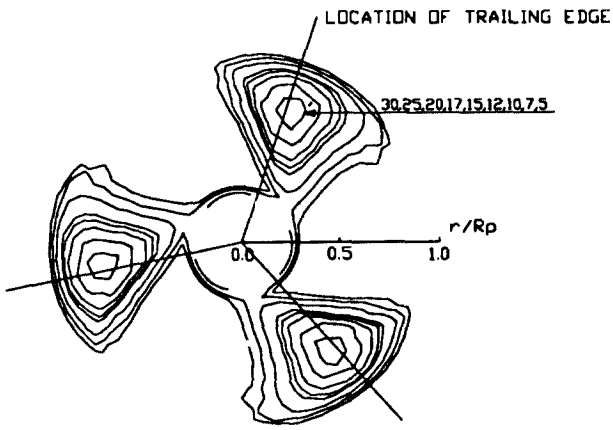

(b) calulated values

Fig. 16 Turbulent kinetic energy distributions at $x/L=0.9835$

was not observed in the simulation. The number of grid point in the present study is not enough to have confidence in the resolution.

Hyun and Patel plotted the velocity component in the plane perpendicular to the constant pitch surface of the propeller, which is to capture the flow structure more accurately. Measured and calculated streamline components of velocity are shown in Fig. 15. It shows the shape and the thickness of the wake center plane and tip vortex formation. Finally the turbulent kinetic energy distribution is shown in Fig. 16. The high value of turbulent kinetic energy is limited within the blade wake and the tip vortex. There is large discrepancy between the calculated and measured contours. The maximum value of kinetic energy was as high as 0.130 at the maximum load radius of the suction surface, where the radial and circumferential gradients of mean velocity are large. Simulated maximum value is 0.030 at the same location. If we remember that the circumferentially averaged distribution of kinetic energy was in accordance with measured one at this section (cf. Fig. 11), the total kinetic energies in the section coincide each other. The layer of turbulent kinetic energy was diffused more across the blade wake in comparison with the measured one.

6. CONCLUSION

Three dimensional viscous flow simulation around the marine propeller was carried out and the results were compared with the available data. The discussion was made mainly in the wake, not on the flow over the blade. The important results and conclusion are summarized below.

(1) The mean velocity and turbulent kinetic energy were reasonably simulated up to the one diameter downstream of the propeller, while there are significant discrepancies in the wake. At the downstream of the wake, the predicted values of turbulent kinetic energy are considerably smaller than the measured values. The standard from of k-ε model may not be adequated for the swirling flow in the downstream.

(2) The structure of viscous wake of the marine propeller, i.e. a tip vortex core formation, the shape of the wake center plane, the location of maximum axial velocity on the suction side, etc. was reasonably simulated. However, the predicted wake was diffused more across the blade in comparison with the measured wake. Furthermore, any conclusion could not be drawn about the structure inside the tip vortex.

(3) The application of viscous analysis for the marine propeller looks promising, however it shows some difficulties in the efficient grid alignment as well as the numerics. Further investigation should be made.

ACKNOWLEDGEMENT

The present work was partially supported from the Turbo and Power Machinery Research Center funded by the Korea Science and Engineering Foundation. Dr. B.S. Hyun kindly provided the measured data file.

REFERENCES

Huang, T.T., Groves, N.C. and Belt, G.S., 1980, "Boundary Layer Flow on an Axisymmetric Body with an Inflected Stern," DTNSRDC Report 801064, David Taylor Research Center, MA..

Hyun, B.S., 1990, "Measurements in the Flow Around a Marine Propeller at the Stern of an Axisymmetric Body," Ph. D. Thesis, The University of Iowa.

Hyun, B.S. and Patel, V.C., 1991 a, "Measurements in the Flow Around a Marine Propeller at the Stern of an Axisymmetric Body, Part 1 : Circumferentially-Averaged Flow," Experiments in Fluids, 11, pp. 33~44.

Hyun, B.S. and Patel, V.C., 1991 b, "Measurements in the Flow Around a Marine Propeller at the Stern of an Axisymmetric Body, Part 2 : Phase-averaged flow," Experiments in Fluids, 11, pp. 105~117.

Kang, S.H., Lee, J.S., Kim, Y.H. and Kim, K.Y., 1992, "Numerical Calculations of the Turbulent Flow through a Controlled Diffusion Compressor Blade in Cascade," Proceeding of ISROMAC-4, Hawaii, U.S.A.

Kang, S.H., Oh, K.J. and Kobayashi,T., 1991, "A Viscous Flow Calculation of the Stern Flow," KSME Journal, 5(1), pp. 36~44.

Oh, K.J. and Kang,S.H., 1992, "Full Scale Reynolds Number

Effects for the Viscous Flow Around the Ship Stern," Computational Mechanics, 9(2).

Patankar, S.V., 1980, Numerical Heat Transfer and Fluid Flow, McGraw-Hill Book Company, New York.

Stern, F. and Kim, H.T., 1990, "Computation of Viscous Flow Around a Propeller-Shaft Configuration with Infinite-Pitch Rectangular Blades," Proc. 5th Int. Conf. Numerical Ship Hydrodynamics, Hiroshima, Japan.